ROYAL SOCIETY
OF CHEMISTRY

PAPER

Check for updates

Tuning electronic and magnetic properties of monolayer α-RuCl₃ by in-plane strain†

F. Iyikanat, [ID] *[a] M. Yagmurcukardes, [ID] [b] R. T. Senger [ID] [ac] and H. Sahin [ID] *[cd]

By employing density functional theory-based methods, the structural, vibrational, electronic, and magnetic properties of monolayer α-RuCl₃ were investigated. It was demonstrated that ferromagnetic (FM) and zigzag-antiferromagnetic (ZZ-AFM) spin orders in the material have very close total energies with the latter being the ground state. We found that each Ru atom possesses a magnetic moment of 0.9 μ_B and the material exhibits strong magnetic anisotropy. While both phases exhibit indirect gaps, the FM phase is a magnetic semiconductor and the ZZ-AFM phase is a non-magnetic semiconductor. The structural stability of the material was confirmed by phonon calculations. Moreover, dynamical analysis revealed that the magnetic order in the material can be monitored *via* Raman measurements of the crystal structure. In addition, the magnetic ground state of the material changes from ZZ-AFM to FM upon certain applied strains. Valence and conduction band-edges of the material vary considerably under in-plane strains. Owing to the stable lattice structure and unique and controllable magnetic properties, monolayer α-RuCl₃ is a promising material in nanoscale device applications.

I Introduction

Nanoscale magnetic materials and their tunable characteristics are important for the design of nanosized controllable magnets that can be utilized in spintronic applications. A large family of two-dimensional (2D) materials are essential for the fundamental studies of magnetism at the 2D limit. As triggered by extraordinary properties observed in graphene,[1–4] other 2D materials such as hexagonal-BN (h-BN),[5] silicene,[6,7] germanene,[8] transition metal dichalcogenides (TMDs),[9–11] and phosphorene[12] have revealed their potential for technological applications in nanoelectronics, optoelectronics, photonics, and spintronics. Among these ultra-thin materials, the most studied one is graphene due to its weak spin–orbit interaction and long spin relaxation lengths.[13] Although pristine graphene is nonmagnetic, nanoribbons and patches of graphene exhibit magnetic properties.[14–18] It was also found that MoS₂ nanosheets with high density of prismatic edges show weak magnetism.[19] These nanosheets exhibit a 2.5% magnetoresistance effect with a Curie temperature of 685 K. It was predicted

that the monolayer forms of pristine VS₂ and VSe₂ exhibit magnetic behavior.[20] The magnetic moment and strength of magnetic coupling strongly depend on the applied strain in these materials. In previous studies, several groups have shown that magnetism in ultra-thin materials can be induced and engineered by applied strain,[21–23] doping by adatoms,[24] and by introducing vacancy defects.[25,26]

As a new member of the layered materials, α-RuCl₃ has attracted considerable attention in recent years due to its unusual magnetic properties.[27] α-RuCl₃ has a layered structure consisting of planes of edge-sharing RuCl₆ octahedra arranged in a slightly distorted honeycomb lattice.[28] The layers in the crystal structure are held together by weak van der Waals forces.[29] Spectroscopic investigations revealed that α-RuCl₃ is a Mott insulator.[30] It was shown that strong electron correlations play an essential role in determining the exact ground state of this material.[31]

In a recent study, Kim *et al.* demonstrated that due to electron correlations, Kitaev interactions arise in 4d-orbitals of α-RuCl₃.[32,33] It was found that the magnetic ground state of α-RuCl₃ is a zigzag-ordered phase. Majumder *et al.* showed that α-RuCl₃ possesses strong magnetic anisotropy and the successive magnetic order at low temperatures could be completely suppressed by applying fields up to 14 T in the honeycomb plane, whereas the magnetic order is robust when the field applied is perpendicular to the crystal plane.[34] It was found that g-factors of α-RuCl₃ are strongly anisotropic.[35] In another study, the signature of a magnetic transition in magnetic susceptibility and specific heat data were observed.[36] It was found that

[a] Department of Physics, Izmir Institute of Technology, 35430, Izmir, Turkey.
  E-mail: fadiliyikanat@iyte.edu.tr
[b] Department of Physics, University of Antwerp, Groenenborgerlaan 171,
  B-2020 Antwerp, Belgium
[c] ICTP-ECAR Eurasian Center for Advanced Research, Izmir Institute of Technology,
  35430, Izmir, Turkey
[d] Department of Photonics, Izmir Institute of Technology, 35430, Izmir, Turkey.
  E-mail: hasansahin@iyte.edu.tr

there is a zigzag type magnetic order in the honeycomb plane in this material. However, stacking disorder along the direction perpendicular to the plane leads to quite low ordering of magnetic moments. Recently, as a first case in halides, exfoliation of α-RuCl$_3$ into monolayers has been reported.[37]

Even though the bulk form of α-RuCl$_3$ was studied very extensively, very little is known about its monolayer form. The aim of the present paper is to determine the structural, electronic, and magnetic ground state of monolayer α-RuCl$_3$ and to investigate the effects of in-plane uniaxial strain on these properties.

The paper is organized as follows: details of the computational methodology are provided in Section II. After the determination of the magnetic ground state, structural, electronic and magnetic properties of the material are described in Section III. The stability of monolayer α-RuCl$_3$ is discussed in Section IV. The effects of anisotropic strain on the characteristic properties of the material are provided in Section V. Then we conclude our results in Section VI.

II Computational methodology

All the calculations were performed using the Vienna *ab-initio* Simulation Package (VASP)[38,39] based on the projector augmented wave (PAW)[40,41] formalism of spin-polarized density functional theory. For the exchange–correlation energy, generalized gradient approximation of the Perdew–Burke–Ernzerhof (GGA-PBE) functional was used.[42] In addition to bare PBE, spin–orbit interactions were included in the electronic calculations. In order to take into account strong correlations between d-orbitals of Ru atoms, the DFT+U method described by Dudarev was used.[43] In this method the on-site Coulomb parameter, U, and the exchange parameter, J, are combined into one parameter, which is $U_{eff} = U - J$. In accordance with a previous study, the effective U parameter was chosen to be U_{eff} = 2 eV.[44] It is important to note that the ground state of the material strongly depends on whether the effective U parameter is included in the geometric optimizations or not. In our calculations, the effective U parameter was taken into consideration not only in electronic calculations but also in structural relaxations.

A plane-wave basis set with a kinetic energy cut-off of 400 eV was used. Γ-Centered k-point mesh was employed with grid sizes of $7 \times 4 \times 1$ and $15 \times 9 \times 1$ for the structural relaxation and the density of states (DOS) calculation, respectively. Bader charge analysis was used to obtain charge transfer between the individual atoms in the crystal structure.[45] The criterion of convergence of energy was chosen as 10^{-5} eV between two ionic steps, and the maximum force allowed on each atom was 10^{-4} eV Å^{-1}. To hinder interactions between the adjacent cells, at least a vacuum spacing of 14 Å was used along the z-direction. DFT plus the long-range dispersion correction (DFT+D2) method was used to calculate nonlocal correlation energies.[46] A Gaussian smearing factor of 0.05 eV was used and the pressures on the unit cell were decreased to a value less than 1.0 k_B in all three directions.

The vibrational properties of all magnetic orders for monolayer α-RuCl$_3$ were calculated in terms of the off-resonant Raman activities of phonon modes at the Γ point. For this purpose, the vibrational phonon modes at the Γ point were calculated using the finite-difference method as implemented in VASP. Each atom in the conventional cell was initially distorted by 0.01 Å and the corresponding dynamical matrix was constructed. Then, the vibrational modes were determined by a direct diagonalization of the dynamical matrix. For these calculations $18 \times 18 \times 1$ Γ centered k-point sampling was used. Once the accurate phonon mode frequencies were obtained at the Γ point, changes in the macroscopic dielectric tensor were calculated with respect to each vibrational mode.

III Electronic and magnetic properties

The determination of the magnetic ground state of monolayer α-RuCl$_3$, in which each Ru atom possesses a magnetic moment of 0.9 μ_B, is essential for a reliable approximation of electronic band dispersion. Four different magnetic configurations are considered such as: ferromagnetic (FM), antiferromagnetic (AFM), zigzag-antiferromagnetic (ZZ-AFM) and stripy. The spin-polarized charge densities of these magnetic configurations are shown in Fig. 1. The conventional cell of monolayer α-RuCl$_3$ comprises 4Ru and 12Cl atoms. The total energy calculations reveal that while the ZZ-AFM state is the ground state, FM, AFM and stripy configurations have 3, 55, and 19 meV per conventional cell higher energies than ZZ-AFM, respectively. Since the total energy of the FM state is quite close to the ground state, we consider only ZZ-AFM and FM states in the rest of the paper.

The calculated lattice parameters and octahedron distances (d_1 and d_2) of ZZ-AFM and FM configurations are provided in Table 1. It is obvious that the different magnetic orders among the Ru atoms change the equilibrium lattice parameters. RuCl$_6$ octahedrons of the material have quite an ordered honeycomb structure in the FM state, and thus the octahedron distances are the same and equal to 3.46 Å for FM. On the other hand, magnetic interactions between Ru atoms of ZZ-AFM lead to dimer formation in the lattice. Ru atoms form dimers by decreasing d_1 to 3.45 Å and increasing d_2 to 3.48 Å for ZZ-AFM. As seen in Fig. 1, each Ru atom interacts with six Cl atoms, half of them from the top Cl-layer and the other half from the bottom Cl-layer. The bond length between Ru and Cl atoms is 2.38 Å for the FM state, whereas that of the ZZ-AFM state varies from 2.37 to 2.39 Å. To investigate the bonding characteristic in monolayer α-RuCl$_3$, Bader charge analysis was used. Our results show that Ru and Cl atoms are covalently bonded. Such a bond is constructed by a charge transfer of $\sim$0.3 e from Ru to Cl.

It is found that each Ru atom in both configurations of α-RuCl$_3$ has a net magnetic moment of 0.9 μ_B. Magnetic anisotropy energy (MAE) of both configurations is also calculated. The MAE is the energy difference between the easy axis magnetization energy (E_{easy}) and the hard axis magnetization energy (E_{hard}),
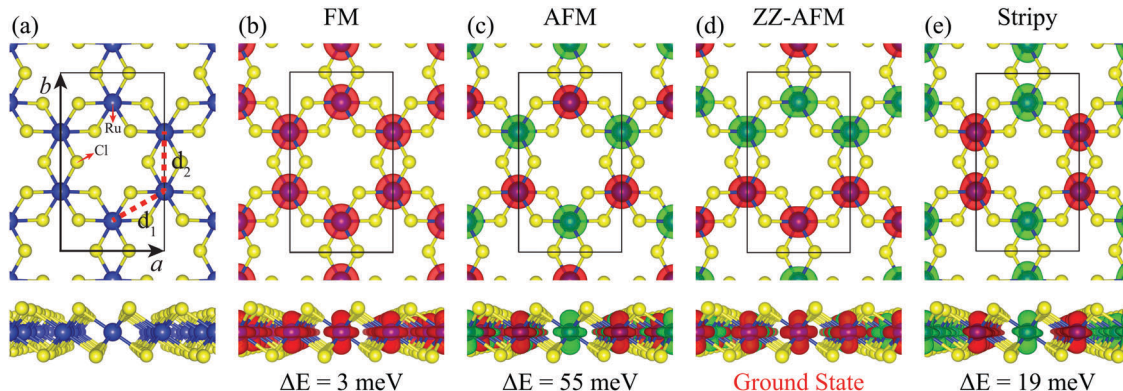
$$\text{MAE} = E_{hard} - E_{easy}.$$

Fig. 1 (a) Top and side views of the geometric structure of monolayer α-RuCl$_3$. Blue and yellow atoms represent Ru and Cl, respectively. Ru–Ru distances are represented as d_1 and d_2. Top and side views of the spin density plot of (b) FM, (c) AFM, (d) ZZ-AFM, and (e) stripy configurations (maintaining the same isosurface value of 0.01 e Å^{-3} for each of the plots). Red and green isosurfaces represent the majority and minority spin densities, respectively.

Table 1 Calculated conventional cell lattice parameters a and b, Ru–Ru distances d_1 and d_2 (which are shown in Fig. 1(a)), the Bader charge transferred between Ru and Cl atoms ρ, absolute magnetic moment per Ru atom μ (Bohr magneton), magnetic anisotropy energy per Ru atom (MAE), and energy band gap E_g

	a (Å)	b (Å)	d_1 (Å)	d_2 (Å)	ρ (e)	μ (μ_B)	MAE (meV)	E_g (eV)
ZZ-AFM	5.97	10.44	3.45	3.48	0.3	0.9	0.80	0.96
FM	6.00	10.38	3.46	3.46	0.3	0.9	0.95	0.69

The spin–orbit interaction is added to the calculations with the following Hamiltonian,

$$H_{SO} = \frac{1}{2r(m_e c)^2}\frac{dV}{dr}\vec{L}\cdot\vec{S},$$

where r is the radial distance from the atom nuclei, m_e is the electron mass, c is the speed of light, V is the potential around the nuclei, and $\vec{L}$ and $\vec{S}$ are the orbital momentum and spin operators, respectively.

As seen in Fig. 1 the origin of magnetization is the electrons in the d-orbital of Ru atoms which is not spherically symmetric. Therefore, magnetic anisotropy is expected in this material. Magnetic anisotropy defines the stability of the magnetization direction against thermal excitations. A large magnetic anisotropy is crucial to preserve magnetic moments from thermal fluctuations. Materials with high magnetocrystalline anisotropy are important in data storage, magnetic sensors, and spintronic applications.

Fig. 2 shows the variations of MAE projected on the sphere for ZZ-AFM and FM configurations. The net magnetic moment of the FM state is 4 μ_B per conventional cell. It is found that the easy-axis for the FM state is parallel to the plane of the material, and the in-plane anisotropy is negligibly small. However, the easy axis direction of the ZZ-AFM state makes a small angle with the plane of the material. Compared to the FM state, the in-plane anisotropy of MAE is observed in the ZZ-AFM state. The energy difference between the easy axis and hard axis of FM and ZZ-AFM states is 0.95 meV per Ru and 0.80 meV per Ru, respectively. Therefore, it is worth noting that although the
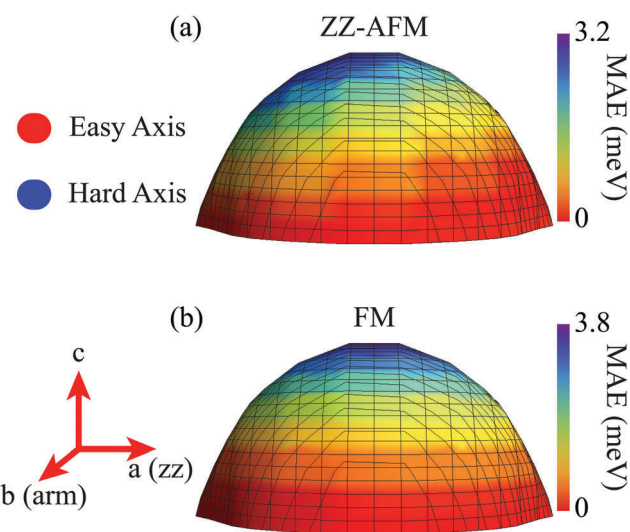

Fig. 2 The variations of MAE values are projected on the sphere for (a) ZZ-AFM and (b) FM configurations.

ZZ-AFM state does not have a net magnetic moment, it has a comparable MAE value with the FM state. The calculated MAE value of α-RuCl$_3$ is larger than that of other 2D materials such as CrF$_3$, CrCl$_3$, CrBr$_3$, and CrI$_3$.[47] Moreover, the MAE of α-RuCl$_3$ is comparable to that of Fe$_3$GeTe$_3$ and FeCo alloys, which are known as materials exhibiting giant magnetic anisotropy.[48,49] We also calculated the Curie temperature of monolayer α-RuCl$_3$ using the Heisenberg model in which the Hamiltonian can be written as

$$H = -J\sum_{ij}\hat{m}_i\hat{m}_j \tag{1}$$

where J is the Heisenberg exchange parameter and $\hat{m}$ is the magnetic moment of each site (μ_B). Only the nearest neighbor exchange interaction is taken into account; thus, the expression for the Heisenberg exchange parameter for our system is $J = E_{ex}/6m^2$, where E_{ex} is the exchange energy per unit cell. It is found that $J = 0.62$ meV. Using the mean field approximation, which is $k_B T_c = 3/2J$, the Curie temperature is found to be 10.8 K.

This journal is © The Royal Society of Chemistry 2018
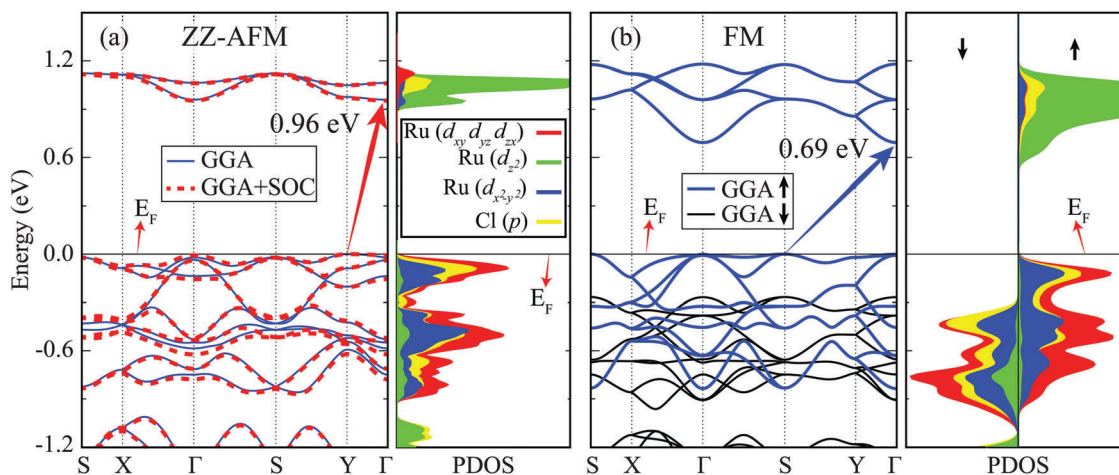
J. Mater. Chem. C, 2018, 6, 2019–2025 | **2021**

Fig. 3 (a) Calculated band dispersions within GGA and GGA+SOC, and partial density of states (PDOS) of the ZZ-AFM state of single-layer α-RuCl$_3$. (b) Calculated band dispersion within GGA, and partial density of states (PDOS) of the FM state of single-layer α-RuCl$_3$. Spin-up (↑) and spin-down (↓) bands are represented as blue and black lines, respectively. The Fermi energy (E_F) level is set to the valence band maximum.

Band dispersions of the ZZ-AFM state based on GGA and GGA+SOC including the U-Hubbard term are shown in Fig. 3(a). As seen in the figure, SOC has a negligible influence on the electronic structure of the material. The ZZ-AFM state is an indirect-gap semiconductor with a calculated band gap of 0.96 eV. The FM state is also an indirect-gap semiconductor; however, the spin-up and spin-down bands are spin-split in both valence and conduction bands (see Fig. 3(b)). The band gap is much larger in the spin-up states than that in the spin-down states. The band gap is 0.69 eV for the spin-up states whereas it is 2.20 eV for the spin-down states. The trends between our results and previously predicted band diagrams are in good agreement with each other.[32,33] Since the bare-GGA generally underestimates the band gap of semiconductors, some deviations are expected in the experimental band gap of the material. While the conduction band minimum (CBM) of both configurations are located at the Γ symmetry point, the valence band maximum (VBM) of ZZ-AFM and FM states resides in the Y and S symmetry points, respectively. The dispersions near the VBM are quite linear for both the cases. This indicates a large effective mass for the holes in this material. It is seen that the valence band edge at the Γ point differs by only 8 meV and 1 meV from the VBM of the ZZ-AFM and FM configurations, respectively. The partial density of states (PDOS) are also calculated for both the magnetic ordering states. It is found that for both the magnetic configurations, CBM is mostly dominated by d$_{z^2}$-orbitals of the Ru atom, whereas VBM is composed of d$_{xy}$, d$_{yz}$, d$_{zx}$ and d$_{x^2-y^2}$-orbitals of the Ru atom and p-orbitals of the Cl atom. Near the VBM, the overlap of PDOS peak positions and shapes of d-orbitals of the Ru atom and p-orbitals of the Cl atom reveal strong coupling between these orbitals.

Fig. 4 Phonon-band structure and corresponding Raman activities of monolayer α-RuCl$_3$ for: (a) FM and (b) ZZ-AFM configurations. The vibrational motion of individual atoms in some prominent Raman active modes is also shown in the right panel.

IV Vibrational properties

For an accurate investigation of the dynamical stability of a material, analysis of the phonon modes provides a reliable
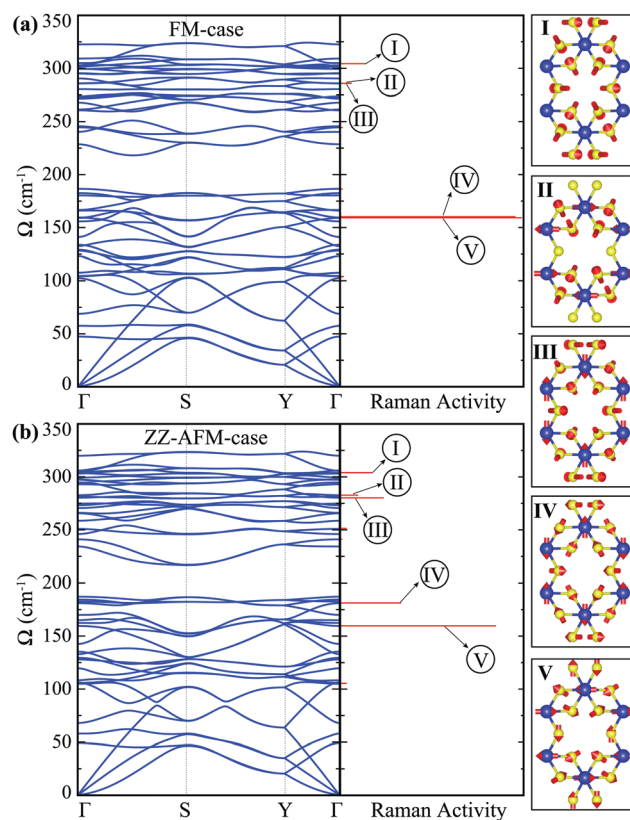
result. We calculate the phonon-band structures based on the small-displacement method as implemented in the PHON code.[50] As seen in the left panel of Fig. 4(a) and (b), both the FM and ZZ-AFM states of monolayer α-RuCl$_3$ are dynamically stable. There are 36 vibrational modes 3 of which are acoustical

phonon branches. Since the geometry of two magnetic phases is slightly different (the in-plane isotropy is broken in ZZ-AFM) phonon-band structures display differences in the peak frequencies of some phonon modes. This can be detected by Raman measurements. As shown in the right panel of Fig. 4(a) and (b), there are 5 prominent Raman active phonon modes for both magnetic orders. Vibrational characteristics of mode-I demonstrate that the Ru atoms are stationary. Since the magnetic interaction occurs between the Ru atoms, mode-I has approximately the same peak frequencies for both cases (305.0 and 304.0 cm^{-1} for FM and ZZ-AFM, respectively). In the other 4 phonon modes, in addition to the vibration of Cl atoms, Ru atoms also contribute to vibration. Therefore, the shift in peak frequencies of these phonon modes is greater. The frequencies of phonon modes II and III are calculated to be 285.9 and 285.7 cm^{-1} in the FM case, respectively. Although they have very close frequencies these modes are non-degenerate. In the case of ZZ-AFM ordering, there is a splitting between modes II and III (the frequencies are 282.7 and 280.3 cm^{-1} for mode-II and III, respectively). In addition to the splitting of the frequencies, there also occurs small phonon softening in the ZZ-AFM case. In fact, a larger splitting occurs between phonon modes IV and V when the ZZ-AFM interaction exists in the crystal. The frequency of phonon mode-IV is calculated to be 159.5 and 181.1 cm^{-1} in FM and ZZ-AFM cases, respectively. This large splitting of the frequency is a strong indication of different magnetic interactions in the crystal. However, the phonon mode-V has exactly the same frequency (159.5 cm^{-1}) in both cases. In addition, as seen in Fig. 4, the Raman activities of phonon modes IV and V are higher in the FM case which can also be a key for the indication of different magnetic interactions in the crystal. Therefore, it can be pointed out that although two magnetic cases have very close total energies (3 meV of difference) their Raman spectra are considerably different.

V Strain application

Formation or synthesis of monolayer crystals by removing the adjacent layer not only leads to dimensional crossover from 3D to 2D behavior of elementary excitons but also increases the sensitivity of the crystal against strain. Soft materials such as $RuCl_3$ may exhibit interesting properties under external strain. Since it is an easy and effective method, strain is often used to manipulate fundamental properties of ultra-thin materials.[20,51–54] Hence, the strain effect on the structural, magnetic, and electronic properties of monolayer α-$RuCl_3$ is investigated in this section.

Fig. 5 shows the in-plane strain-dependent total energy differences of ZZ-AFM and FM configurations with respect to the unstrained case. Using the rectangular conventional cells as shown in Fig. 1(b) and (d) uniaxial strain is applied along the zigzag (ε_{zig}) and armchair (ε_{arm}) directions. The lattice parameters of the conventional cells for compressive and tensile strains are changed up to 3%. The conventional cell vector perpendicular to the direction of the applied strain and atomic positions are fully relaxed for each strained case.

As seen in Fig. 5(a), the magnetic ground state of monolayer α-$RuCl_3$ experiences a phase transition from ZZ-AFM to FM below 1% tensile strain along the zigzag direction. While the magnetic ground state of the material is still FM, energy differences between FM and ZZ-AFM states increase with the increase of tensile strain. However, applying compressive strain
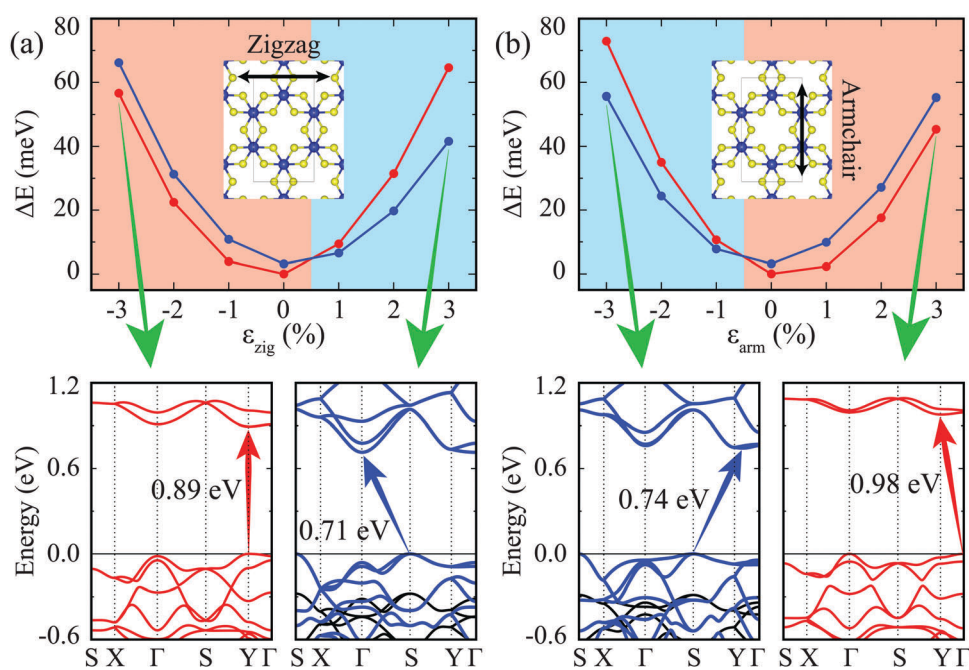

Fig. 5 The variations of the total energy differences and ground state electronic band dispersions of ZZ-AFM and FM phases as a function of in-plane strain along (a) zigzag (ε_{zig}) and (b) armchair (ε_{arm}) directions. Blue and red shaded regions delineate the FM and ZZ-AFM regions, respectively.

along the zigzag direction does not produce such a change in the magnetic ground state of the material and energy differences between ZZ-AFM and FM states are almost unchanged with the increase in compressive strain. Fig. 5(b) clearly shows that the opposite scenario occurs when the uniaxial strain is applied along the armchair direction. The magnetic ground state changes from ZZ-AFM to FM below 1% compressive strain. Therefore, it is obvious that applying uniaxial strain is an easy and practical method to modulate magnetic ordering in this material.

Since the applied in-plane strain significantly modifies interatomic distances and distribution of electrons, it can induce prominent variations in the electronic characteristics of the material as well. Hence, in this section, the modifications in the electronic structure of monolayer α-RuCl$_3$ caused by the in-plane strain are discussed. Lower panels in Fig. 5(a) and (b) present the evolution of the electronic band dispersions of ZZ-AFM and FM configurations under uniaxial strains, respectively. We find significant strain-induced changes in the VBM and CBM. The ground state of the material is ZZ-AFM and it is a semiconductor with a direct gap at the Y symmetry point when 3% compressive strain is applied along the zigzag direction. With the increase of tensile strain up to 3% along the same direction, the valence band at the S point moves upwards in energy, and the FM phase exhibits an indirect gap $(SS \rightarrow \Gamma)$ character. The material exhibits the FM configuration with an indirect gap $(SS \rightarrow$ between the $Y-\Gamma)$ when 3% compressive strain is applied along the armchair direction. The ground state of the material is ZZ-AFM with an indirect band gap $(\Gamma \rightarrow Y)$ under 3% tensile strain along the armchair direction.

VI Conclusions

In summary, we performed first-principles calculations in order to investigate the structural, vibrational, electronic, and magnetic properties of monolayer α-RuCl$_3$ and the effects of in-plane strain on these properties. Magnetic ordering in the ground state of the material is ZZ-AFM, with an FM phase present just 3 meV above the ground state. It was found that both magnetic configurations possess strong magnetic anisotropy. Our calculations revealed that both ZZ-AFM and FM phases are indirect gap semiconductors. The calculated phonon dispersion curves showed that both phases are dynamically stable. It was also predicted that since the phonon modes of the two phases exhibit substantial differences, the magnetic state of the material can be monitored by Raman measurements.

Moreover, our calculations revealed that the magnetic ground state of the material can be readily tuned by certain in-plane strains. The band gaps of ZZ-AFM and FM states remain almost unchanged under in-plane strain, whereas significant modifications occur at the valence and conduction band edges. With its strain-dependent magnetic properties, monolayer α-RuCl$_3$ is a promising material for future spintronic applications.

Conflicts of interest

There are no conflicts to declare.

Acknowledgements

References

1 K. S. Novoselov, A. K. Geim, S. V. Morozov, D. Jiang, Y. Zhang, S. V. Dubonos, I. V. Grigorieva and A. A. Firsov, *Science*, 2004, **306**, 666.

2 A. K. Geim and K. S. Novoselov, *Nat. Mater.*, 2007, **6**, 183.

3 S. Y. Zhou, D. A. Siegel, A. V. Fedorov and A. Lanzara, *Phys. Rev. Lett.*, 2008, **101**, 086402.

4 S. Stankovich, D. A. Dikin, G. H. B. Dommett, K. M. Kohlhaas, E. J. Zimney, E. A. Stach, R. D. Piner, S. T. Nguyen and R. S. Ruoff, *Nature*, 2006, **442**, 282.

5 K. K. Kim, A. Hsu, X. Jia, S. M. Kim, Y. Shi, M. Hofmann, D. Nezich, J. F. R. Nieva, M. Dresselhaus, T. Palacios and J. Kong, *Nano Lett.*, 2012, **12**, 161.

6 P. Vogt, P. D. Padova, C. Quaresima, J. Avila, E. Frantzeskakis, M. C. Asensio, A. Resta, B. Ealet and G. L. Lay, *Phys. Rev. Lett.*, 2012, **108**, 155501.

7 A. Fleurence, R. Friedlein, T. Ozaki, H. Kawai, Y. Wang and Y. Takamura, *Phys. Rev. Lett.*, 2012, **108**, 245501.

8 Z. Ni, Q. Liu, K. Tang, J. Zheng, J. Zhou, R. Qin, Z. Gao, D. Yu and J. Lu, *Nano Lett.*, 2012, **12**, 113.

9 B. Radisavljevic, A. Radenovic, J. Brivio, V. Giacometti and A. Kis, *Nat. Nanotechnol.*, 2011, **6**, 147.

10 M. Chhowalla, H. S. Shin, G. Eda, L.-J. Li, K. P. Loh and H. Zhang, *Nat. Chem.*, 2013, **5**, 263.

11 M. Yagmurcukardes, C. Bacaksiz, R. T. Senger and H. Sahin, *2D Mater.*, 2017, **4**, 035013.

12 H. Liu, A. T. Neal, Z. Zhu, Z. Luo, X. Xu, D. Tománek and P. D. Ye, *ACS Nano*, 2014, **8**, 4033.

13 D. Pesin and A. H. MacDonald, *Nat. Mater.*, 2012, **11**, 409.

14 M. Golor, S. Wessel and M. J. Schmidt, *Phys. Rev. Lett.*, 2014, **112**, 046601.

15 J. Jung and A. H. MacDonald, *Phys. Rev. B: Condens. Matter Mater. Phys.*, 2009, **79**, 235433.

16 T. Wassman, A. P. Seitsonen, A. M. Saitta, M. Lazzeri and F. Mauri, *Phys. Rev. Lett.*, 2008, **101**, 096402.

17 H. Sahin, R. T. Senger and S. Ciraci, *J. Appl. Phys.*, 2010, **108**, 074301.

18 M. Ezawa, *Phys. Rev. B: Condens. Matter Mater. Phys.*, 2007, **76**, 245415.

19 J. Zhang, J. M. Soon, K. P. Loh, J. Yin, J. Ding, M. B. Sullivan and P. Wu, *Nano Lett.*, 2007, **7**, 2370.

2024 | *J. Mater. Chem. C*, 2018, **6**, 2019–2025

This journal is © The Royal Society of Chemistry 2018

20 Y. Ma, Y. Dai, M. Guo, C. Niu, Y. Zhu and B. Huang, *ACS Nano*, 2012, **6**, 1695.

21 S. Yang, C. Wang, H. Sahin, H. Chen, Y. Li, S.-S. Li, A. Suslu, F. M. Peeters, Q. Liu, J. Li and S. Tongay, *Nano Lett.*, 2015, **15**, 1660.

22 Y. Zhou, Z. Wang, P. Yang, X. Zu, L. Yang, X. Sun and F. Gao, *ACS Nano*, 2012, **6**, 9727.

23 H. Zheng, B. Yang, D. Wang, R. Han, X. Du and Y. Yan, *Appl. Phys. Lett.*, 2014, **104**, 132403.

24 A. V. Krasheninnikov, P. O. Lehtinen, A. S. Foster, P. Pyykkö and R. M. Nieminen, *Phys. Rev. Lett.*, 2009, **102**, 126807.

25 O. V. Yazyev and L. Helm, *Phys. Rev. B: Condens. Matter Mater. Phys.*, 2007, **75**, 125408.

26 M. M. Ugeda, I. Brihuega, F. Guinea and J. M. G. Rodrguez, *Phys. Rev. Lett.*, 2010, **104**, 096804.

27 S. Sarikurt, Y. Kadioglu, F. Ersan, E. Vatansever, O. Ü. Aktürk, Y. Yüksel, Ü. Akinci and E. Aktürk, *Phys. Chem. Chem. Phys.*, 2018, **20**, 997.

28 J. M. Fletcher, W. E. Gardner, A. C. Fox and G. Topping, *J. Chem. Soc. A*, 1967, 1038.

29 I. Pollini, *Phys. Rev. B: Condens. Matter Mater. Phys.*, 1994, **50**, 2095.

30 I. Pollini, *Phys. Rev. B: Condens. Matter Mater. Phys.*, 1996, **53**, 12769.

31 K. Plumb, J. Clancy, L. Sandilands, V. V. Shankar, Y. Hu, K. Bruch, H.-Y. Kee and Y.-J. Kim, *Phys. Rev. B: Condens. Matter Mater. Phys.*, 2014, **90**, 041112.

32 H.-S. Kim, V. V. Shankar, A. Catuneanu and H.-Y. Kee, *Phys. Rev. B: Condens. Matter Mater. Phys.*, 2015, **91**, 241110.

33 L. J. Sandilands, Y. Tian, A. A. Reijnders, H.-S. Kim, K. W. Plumb, Y.-J. Kim, H.-Y. Kee and K. S. Bruch, *Phys. Rev. B: Condens. Matter Mater. Phys.*, 2016, **93**, 075144.

34 M. Majumder, M. Schmidt, H. Rosner, A. A. Tsirlin, H. Yasuoka and M. Baenitz, *Phys. Rev. B: Condens. Matter Mater. Phys.*, 2015, **91**, 180401.

35 Y. Kubota, H. Tanaka, T. Ono, Y. Narumi and K. Kindo, *Phys. Rev. B: Condens. Matter Mater. Phys.*, 2015, **91**, 094422.

36 J. A. Sears, M. Songvilay, K. W. Plumb, J. P. Clancy, Y. Qiu, Y. Zhao, D. Parshall and Y.-J. Kim, *Phys. Rev. B: Condens. Matter Mater. Phys.*, 2015, **91**, 144420.

37 D. Weber, L. M. Schoop, V. Duppel, J. M. Lippmann, J. Nuss and B. V. Lotsch, *Nano Lett.*, 2016, **16**, 3578.

38 G. Kresse and J. Hafner, *Phys. Rev. B: Condens. Matter Mater. Phys.*, 1993, **47**, 558.

39 G. Kresse and J. Furthmuller, *Phys. Rev. B: Condens. Matter Mater. Phys.*, 1996, **54**, 11169.

40 G. Kresse and D. Joubert, *Phys. Rev. B: Condens. Matter Mater. Phys.*, 1999, **59**, 1758.

41 P. E. Blöchl, *Phys. Rev. B: Condens. Matter Mater. Phys.*, 1994, **50**, 17953.

42 J. P. Perdew, K. Burke and M. Ernzerhof, *Phys. Rev. Lett.*, 1996, **77**, 3865.

43 S. L. Dudarev, G. A. Botton, S. Y. Savrasov, C. J. Humphreys and A. P. Sutton, *Phys. Rev. B: Condens. Matter Mater. Phys.*, 1998, **57**, 1505.

44 H.-S. Kim and H.-Y. Kee, *Phys. Rev. B*, 2016, **93**, 155143.

45 G. Henkelman, A. Arnaldsson and H. Jonsson, *Comput. Mater. Sci.*, 2006, **36**, 354.

46 S. Grimme, *J. Comput. Chem.*, 2006, **27**, 1787.

47 W.-B. Zhang, Q. Qu, P. Zhu and C.-H. Lam, *J. Mater. Chem. C*, 2015, **3**, 12457.

48 H. L. Zhuang, P. R. C. Kent and R. G. Henning, *Phys. Rev. B: Condens. Matter Mater. Phys.*, 2016, **93**, 134407.

49 T. Burkert, L. Nordström, O. Eriksson and O. Heinonen, *Phys. Rev. Lett.*, 2004, **93**, 027203.

50 D. Alfè, *Comput. Phys. Commun.*, 2009, **180**, 2622.

51 H. Sahin, S. Cahangirov, M. Topsakal, E. Bekaroglu, E. Akturk, R. T. Senger and S. Ciraci, *Phys. Rev. B: Condens. Matter Mater. Phys.*, 2009, **80**, 155453.

52 F. Iyikanat, B. Akbali, J. Kang, R. T. Senger, Y. Selamet and H. Sahin, *J. Phys.: Condens. Matter*, 2017, **29**, 485302.

53 N. Levy, S. A. Burke, K. L. Meaker, M. Panlasigui, A. Zettl, F. Guinea, A. H. Castro Neto and M. F. Crommie, *Science*, 2010, **329**, 544.

54 G. Gui, J. Li and J. Zhong, *Phys. Rev. B: Condens. Matter Mater. Phys.*, 2008, **78**, 075435.

This journal is © The Royal Society of Chemistry 2018

J. Mater. Chem. C, 2018, **6**, 2019–2025 | **2025**